Targeting the metabolic response to statin-mediated oxidative stress produces a synergistic anti-tumor response

Grace H. McGregor[1,2], Andrew D. Campbell[1], Sigrid K. Fey[1,2], Sergey Tumanov[1,2], David Sumpton[1], Giovanny Rodriguez Blanco[1], Gillian Mackay[1], Colin Nixon[1], Alexei Vazquez[1,2], Owen J. Sansom[1,2,#], Jurre J. Kamphorst[1,2,3,#,*]

[1] Cancer Research UK Beatson Institute, Garscube Estate, Switchback Road, Glasgow, G61 1BD, UK.

[2] Institute of Cancer Sciences, University of Glasgow, Garscube Estate, Switchback Road, Glasgow, G61 1QH, UK.

[#] Senior authors

* Corresponding author: Jurre Kamphorst, Ph.D: jurre.kamphorst@glasgow.ac.uk

Cancer Research UK Beatson Institute

Garscube Estate

Switchback Road

Bearsden

Glasgow

G61 1BD

+44(0) 141 330 3953

[3] Secondary address: Rheos Medicines Inc,

38 Sidney Street

Cambridge, 02139 MA

jkamphorst@rheosrx.com

+1 857 777 4138

Running Title: MEK inhibition synergizes with statins for cancer treatment

Keywords

Cholesterol, coenzyme Q, mevalonate pathway, redox stress, statin

Conflicts of Interest

J.J.K. is currently an employee and a shareholder of Rheos Medicines, Inc.

Word Count: 9518

Figure Number: 5

Abstract

Statins are widely prescribed inhibitors of the mevalonate pathway, acting to lower systemic cholesterol levels. The mevalonate pathway is critical for tumorigenesis and is frequently upregulated in cancer. Nonetheless, reported effects of statins on tumor progression are ambiguous, making it unclear if statins, alone or in combination, can be used for chemotherapy. Here, using advanced mass spectrometry and isotope tracing, we showed that statins only modestly affected cancer cholesterol homeostasis. Instead, they significantly reduced synthesis and levels of another downstream product, the mitochondrial electron carrier coenzyme Q, both in cultured cancer cells and tumors. This compromised oxidative phosphorylation, causing severe oxidative stress. To compensate, cancer cells upregulated antioxidant metabolic pathways, including reductive carboxylation, proline synthesis, and cystine import. Targeting cystine import with an xCT transporter-lowering MEK inhibitor, in combination with statins, caused profound tumor cell death. Thus, statin-induced ROS production in cancer cells can be exploited in a combinatorial regimen.

Statement of Significance

Cancer cells induce specific metabolic pathways to alleviate the increased oxidative stress caused by statin treatment, targeting one of these pathways synergizes with statins to produce a robust anti-tumor response.

Introduction

The mevalonate pathway plays an important role in cellular and systemic physiology, with downstream pathways contributing to the proper functioning of a diverse set of biological processes. Synthesis of mevalonate occurs by concatenating 3 acetyl-CoA molecules, followed by a reduction step by the enzyme HMG-CoA reductase. Mevalonate is then subject to further phosphorylation and decarboxylation steps, together catalyzing the production of 5-carbon isoprenoid molecules, three of which are used to synthesize a 15-carbon farnesyl pyrophosphate (FPP) molecule (Fig.1A). Isoprenoids and FPP feed into separate downstream pathways to produce a variety of biomolecules. These are (I) dolichols, which are made up of varying numbers of isoprene units and act as anchors for glycosylation structures, (II) prenyl units for protein prenylation, enabling their anchoring into membranes (1), (III) coenzyme Q (CoQ), or ubiquinone, an essential electron carrier in the electron transport chain (2), and (IV) cholesterol. Cholesterol is arguably the best studied product of the mevalonate pathway, and is an important lipid that acts as a structural component of mammalian cell membranes and a precursor for the synthesis of steroid hormones, bile acid, and vitamin D (3).

Although cholesterol contributes to a variety of important physiological processes, excess levels (hypercholesterolemia) are often observed in individuals with metabolic syndrome, and it is strongly linked to cardiovascular disease (4). This has spurred significant interest into potential pharmacological interventions, leading to the development of statins. These are a class of drugs that inhibit the rate-limiting enzyme producing mevalonate, HMG-CoA reductase (HMGCR), and are thought to exert their beneficial effect by normalizing systemic cholesterol levels. Due to their

favorable efficacy and safety profiles, statins are now amongst the most widely prescribed medicines in the clinic (5).

In recent years there have been many reports linking upregulated activity of the mevalonate and downstream metabolic pathways to cancer development and progression (6,7). For example, in breast cancer it was found that high HMGCR and additional mevalonate pathway gene transcript levels correlated with poor prognosis (6). Likewise, comparison of pancreatic ductal adenocarcinoma (PDAC) and normal pancreas tissue revealed strongly deregulated cholesterol metabolism (8). In addition, it was recently shown that p53 represses the mevalonate pathway and this is one mechanism by which it suppresses tumor development (9). Finally, a commonly occurring driver oncogene, Ras, is prenylated to facilitate its localization to the inside of the plasma membrane. This has been shown to co-operate with increased HMGCR levels to promote transformation (6).

Despite the clear dysregulation of the mevalonate pathway in a variety of cancer types, robust evidence for a therapeutic benefit of statin treatment remains, limited to only a subset of cancer types. Statin use in combination with androgen-deprivation therapy increased time to progression in prostate cancer (10). Similarly in breast cancer, statin use post diagnosis led to a reduced risk of recurrence, although the largest increase was observed when statin use was combined with angiotensin receptor blocker treatment (11). Notably, in the subset of cancers where statins do appear to be effective, this cannot merely be attributed to their effect on protein prenylation (12), indicating that other parts of the mevalonate and downstream pathways contribute to tumorigenesis and could be blocked to achieve clinical benefit.

This discrepancy between upregulated activity of the mevalonate and branching pathways, and the limited clinical effect of statins in most cancer types, suggested to us that cells may be able to adapt their metabolism in response to statin treatment. Here, we performed a comprehensive stable isotope tracing study with both ^{13}C and ^{2}H tracers, to determine which branches of mevalonate metabolism are active in cancer cells and tumors, and how they may be affected by statin treatment. This led to the finding that biosynthesis of coenzyme Q (CoQ) is very pronounced in cultured cells and in tumors. CoQ depletion due to statin treatment causes reduced oxidative phosphorylation and significantly elevated ROS production. Cancer cells in turn boost redox-active metabolic pathways to alleviate ROS levels, with increased cystine import for glutathione production among the strongest responses. While statins on their own had modest cytostatic effects, combination with a MEK-inhibitor (AZD6244), which lowers *xCT* cystine transporter levels, led to synergistic induction of cancer cell death. Thus statins cause metabolic vulnerabilities, and targeting these in a combination treatment paradigm elicits powerful anti-tumor effects.

Methods

Cell culture

KPC mouse cells originally derived from *Pdx1-Cre; Kras$^{G12D/+}$; Trp53$^{R172H/+}$* (KPC) mice (C57BL/6J background), were kindly provided by Dr Jennifer Morton. MIA PaCa-2 PDAC cells were purchased from the American Type Culture Collection. The PC3 prostate cancer cell line was kindly provided by Dr Hing Leung. All cells were routinely passaged in Dulbecco's Modified Eagle Medium (DMEM, Sigma) with 25 mM glucose and 2 mM L-glutamine, supplemented with 5% (v/v) serum (FBS;

Sigma) (base medium). Cells were split at 80% confluence and checked for mycoplasma every 6 weeks using a luciferase based Mycoalert Mycoplasma detection assay (Lonza). Cell lines were authenticated by extracting genomic DNA (Qiagen kit), carrying out Multiplex PCR using GENE PRINT 10 (Promega) and running samples on a 31/30 XL Genetic Analyzer. Cells were plated for experiments 2 passages after thawing and each biological replicate was separated by one passage thereafter. 24 h prior to experiment, cells were plated in 12-well plates, to reach 80% confluency at end point. Experiments were performed in DMEM (experiment medium) supplemented with 2% or 5% dialyzed FBS (DFBS, Sigma) and as indicated with the following nutrients: 10 mM [$U^{13}C$]-glucose (Cambridge isotopes) and/or 2 mM [$U^{13}C$]-glutamine (Sigma), or unlabeled glucose and glutamine at same concentrations. Simvastatin, pitavastatin and atorvastatin (all Sigma) were used at 2 μM concentration, and AZD6244 was used at 250 nM. Rescue experiments were performed using mevalonolactone (Sigma), N-acetyl cysteine (Sigma), mevalonolactone-(methyl-^{13}C) (Sigma) or $^{13}C_9$-L-Tyrosine (Sigma) in experimental quantification medium. Cell numbers were determined using a CASY Cell Counter (Roche).

Cellular experiments

Cells were first plated in 12-well plates in base medium for 24 h, and thereafter medium was replaced to the indicated experiment medium and cells cultured for 48 h for small molecule metabolites, CoQ and dolichol experiments, and 72 h for cholesterol experiments. Cells were cultured in experiment medium for 48 h for cell counting assays and rescue experiments.

Mice

Animal work was performed under Home Office license (70-8645) with ethical approval from the University of Glasgow Animal and Ethical Review board (AWERB). Mice were given access to standard diet and water *ad libitum* in conventional cages. All mouse work was conducted in accordance with ARRIVE guidelines. KPC mice, previously described (13), were genotyped by Transnetyx (Cordoba, TN, USA), were monitored at least 3 times per week, and put on indicated treatment when pancreatic malignancy was confirmed by abdominal palpitation. Mice were sacrificed after 7 days of treatment. Adult mice of both sexes were randomly assigned to cohorts.

Mouse treatment

Upon pancreatic malignancy confirmation, mice were randomly assigned to cohorts. Drug treatment began on the same day as deuterated water supplementation (see below). Mice were given either a daily oral gavage of 100 µL simvastatin vehicle (0.5% methyl cellulose/5% DMSO), simvastatin (50 mg/kg in 0.5% methyl cellulose/5% DMSO) or a twice daily oral gavage of AZD6244 (25 mg/kg 0.5% HPMC + 0.1% Tween-80), or an AZD6244 gavage along with a simvastatin gavage, for 7 days.

$^{2}H_2O$ tracing in mice

Mice were fasted for 6 h prior to termination. Mice were first given an intraperitoneal bolus injection of 0.035 mL/g 0.9% NaCl $^{2}H_2O$, made up using 0.9 g NaCl in 100 mL $^{2}H_2O$ and sterile filtered. Mice were then provided with 8% $^{2}H_2O$ in the drinking water for 7 days. A previously performed time-course analysis demonstrated that steady

state ^{2}H enrichment of approximately 5% of body water was achieved after 5 days, in agreement with results published by others (14).

Analysis of $^{2}H_2O$ enrichment in body water

Plasma was taken at end point and deuterium enrichment in body water was determined via deuterium acetone exchange as described (15,16).

Tissue homogenization

Mouse tissue samples were snap frozen and homogenized in a Cryocooler^{TM} (OPS Diagnostics). A mass of 5-10 mg of tissue was then weighed and vortexed for 15 min at 4^{o}C at 3000 rpm in the appropriate extraction buffer and internal standards (as described below).

Cholesterol extraction and derivatization from cells, medium and tissues

For cellular extracts, at the time of extraction cells were first washed 3x with1 mL 4°C PBS before 700 µL 4°C extraction buffer (1:9 v/v water: methanol) was added. Plates were incubated for 5 min at 4°C before being scraped into HPLC vials and 20 µL of lathosterol (100 ng/µL) internal standard added.

For media extracts, samples were centrifuged at 16,100 g for 5 min at 4°C to remove cell debris and 500 µL supernatant vortexed for 15 min at 3000 rpm at 4°C with 500 µL 1:1 v/v chloroform: methanol and 20 µL of lathosterol (100 ng/µL, Sigma) internal standard. Samples were centrifuged at 16,100g for 5 min at 4°C, the bottom chloroform layer extracted, transferred to an HPLC vial and dried under N_2. Samples were resuspended in 750 µL cold extraction buffer (1:9 v/v water: methanol). For

tissue, 700 µL 4°C extraction buffer and 20 µL of lathosterol (as an internal standard) was used as detailed in tissue extraction.

All samples (cell extracts, medium, tissue) were saponified by heating for 60 min at 80°C with 75 µL of 10 M NaOH to obtain the total cholesterol pool. Upon cooling to room temperature, 200 µL water was added, followed by 500 µL n-hexane. Vials were vortexed for 5 min at 3000 rpm, and the upper hexane layer transferred to an autosampler vial. The n-hexane extraction was repeated and samples dried under N_2. Samples were reconstituted in 50 µL dry pyridine and 50 µL N-Methyl-N-(trimethylsilyl) trifluoroacetamide (MSTFA, Sigma) silylation agent added. Samples were heated at 60°C for 60 min before cooling and immediate analysis by GC-MS.

Dolichol and CoQ extraction

At time of extraction, cells were placed on ice and washed 3 times in 1 mL cold PBS before 750 µL extraction buffer (1:1 v/v PBS: methanol) was added to cells and scraped into 1.5 mL Eppendorf tubes and 500 µL chloroform added. Similarly, for tissues following homogenization as detailed above, 750 µL extraction buffer and then 500 µL chloroform added was added to sample. For all samples, 50 µL 1 mg/mL methanolic butylated hydroxytoluene (BHT, Sigma); SPLASH lipidomix internal standard mix (Avanti Polar Lipids) at 1 µL per 5 mg tissue/10^5 cells and $^2H_9$-CoQ_{10} (Sigma) at 500 ng/mL per 5 mg tissue/10^5 cells was added. Samples were centrifuged at 10,000 g for 5 min before the lower chloroform layer was extracted and dried under N_2. Samples were reconstituted in 1:1 v/v methanol: chloroform at 100 µL/10^5 cells or 0.2 mL/mg tissue and stored at -20°C until LC-MS analysis.

Metabolite extraction

Intracellular metabolite extraction was performed as follows: on ice, cells were washed 3x 1 mL in cold PBS before 500 µL 4°C extraction buffer (methanol, acetonitrile, and water (5:3:2) v/v) was added. After 5 min cells were scraped into Eppendorf tubes and shaken for 15 min at 3000 rpm at 4°C. Tubes were centrifuged at 16,100 g for 5 min at 4°C and the supernatants were transferred into HPLC vials. Vials were stored at -80°C prior to LC-MS analysis.

Media samples were centrifuged at 16,100 g for 5 min at 4°C to remove cell debris and the supernatant vortexed for 15 min at 3000 rpm at 4°C with cold extraction buffer (methanol, acetonitrile, and water (50:30:20 v/v). Samples were centrifuged at 16,100 g for 5 min at 4°C, and the supernatants were transferred into HPLC vials. In addition, a pooled sample of supernatants was created. A series of standard curves were created with pooled samples spiked with increasing concentrations of [$U^{13}C$]-labeled glucose, lactate, glutamate and glutamine, which were used to determine the concentration of glucose, lactate, glutamate and glutamine in media samples. For cystine, peak area was used for a relative concentration to be calculated.

Tissues were reconstituted in extraction buffer (methanol, acetonitrile, and water, 50:30:20 v/v) at 5 mL/mg tissue.

Acetone analysis by GC-MS

Acetone was analyzed using an Agilent 7890B GC system coupled to a 7000 Agilent Triple Quadrupole GC-MS system, with a Phenomenex ZB-1701 column (30 m × 0.25 mm × 0.25 µm). An initial temperature of 40 °C was set to increase at 10

°C/min up to 100°C, held for 0 min. The instrument was operated in split mode (220:1) in the electron impact mode, 70eV.

Cholesterol analysis by GC-MS

Cholesterol was analyzed using an Agilent 7890B GC system coupled to an Agilent 7000 Triple Quadrupole GC-MS system which was operating in a single quadrupole mode, with a Phenomenex ZB-1701 column (30 m × 0.25 mm × 0.25 µm). An initial temperature of 200 °C was set to increase at 20 °C/min up to 280 °C, held for 9 min. The instrument was operated in splitless mode in the electron impact mode, 70eV, for quantification and 50eV for labeling experiments. Cholesterol was quantified and isotope labeling pattern analyzed using Mass Hunter B.06.00 software (Agilent). Cholesterol and lathosterol internal standard peak areas were extracted from mass-to-charge ratio (m/z) 458 for both. Cholesterol was normalized to the internal standard, and a standard curve was used to quantify mg cholesterol per sample.

CoQ and dolichol analysis by LC-MS

LC-MS analysis was performed as described in (17). CoQ was analyzed in positive mode using spray voltage 3 kV. Full MS (scan range 300-1600 m/z) was used at 70 000 resolution with 10^6 automatic gain control and a maximum injection time of 250 ms. For CoQ quantification, XCalibur Software (Thermo) was used to analyze peak height of CoQ_9, CoQ_{10} and $^2H_9$-CoQ_{10} internal standard. Similarly, for dolichols, peak height of dolichol-19 in dolichol internal standard mix (Avanti) was analyzed. Peak heights were normalized against both the internal standard and cell number.

Metabolite analysis by LC-MS

This was performed as described in (18). Peak areas were determined using Thermo TraceFinder software. Metabolites were identified by a combination of exact masses of ions and retention times. This was validated using commercial standards of all detected metabolites run on the system prior to analysis. Peak areas were normalized to cell number.

Body water $^{2}H_2O$ enrichment calculations

Acetone was quantified and isotope labeling pattern analyzed using Mass Hunter B.06.00 software (Agilent). Mass isotopologs 58 and 59 were integrated and their ratio compared to a standard curve to quantify plasma $^{2}H_2O$ enrichment, as described (15,16).

Cholesterol, CoQ and dolichol ^{13}C and ^{2}H tracing calculations

For both [U^{13}C]-glucose/glutamine and $^{2}H_2O$ CoQ and dolichol tracing MAVEN software (19) was used. For cholesterol, Mass Hunter B.06.00 software was used. Peak area for each isotope was extracted and natural abundance isotope correction performed using an in-house generated algorithm.

For ^{13}C mass isotopolog distributions, calculation of fraction newly synthesized cholesterol, dolichol and CoQ was calculated by dividing each isotopolog by the sum of all isotopologs. Calculation of the fraction newly synthesized cholesterol, dolichol and CoQ from *in vivo* $^{2}H_2O$ experiments was performed according to Lee et al (20, 21).

XF cell mito stress analysis

Oxygen consumption rate was determined using an XF^e96 extracellular flux analyzer (Seahorse Agilent Technologies). Mitochondrial respiratory capacity was determined using XF Cell Mito Stress Kit (Agilent Technologies). 24 h prior to analysis, cells were seeded in 5% dFBS supplemented base medium containing 10 mM glucose and 2 mM glutamine and the indicated drugs or DMSO control. 1 h prior to assay, media was replaced with Seahorse media containing 1% dFBS, 10 mM glucose and 2 mM glutamine and indicated drugs/DMSO, pH 7.4. During the assay, 1 µM oligomycin A, 1 µM FCCP, and 0.5 µM rotenone/antimycin A were sequentially added.

NRF2 Knock-down

Cells were passaged 12 h prior to transfection with RNAiMAX (Invitrogen) and siRNA: siGENOME non-targeting control pool (Dharmacon), NRF2 (Nfe212) (Qiagen, SI01326815, SI01326822), according to the vendor's protocol. After 48 h cells were plated and treated as described.

Synergy Assay

Cells were plated in 24 well plates in base media for 24 h, thereafter media was replaced with base media plus drug or control (DMSO). Simvastatin was used at: 0.5, 1, 2, 4, 8 µM. AZD6244 was used at 0.25, 1, 2, 5, 10, 15, 20 µM. A combinatorial matrix of these concentrations was then tested. An Incucyte Zoom (Essen Bioscience) was used to image wells and confluency after 96 h was determined using Incucyte Zoom software (Essen Bioscience). Confluency data was normalized to the vehicle (DMSO) condition. For each drug alone, using Microsoft Excel, the

confluency curve was fitted to a cubic equation. The cubic equation was then used to create a lookup table of percent inhibition vs drug concentration. The IC_X for a given X was then obtained finding the X value in the percent inhibition column and retrieving the associated drug concentration. For a given X and drug concentrations D_1 and D_2, the drug combination index (CI) was then calculated as described by Chou-Talalay (22), using the following equation:

$$CI = \frac{D_A}{IC_{x,A}} + \frac{D_B}{IC_{x,B}}$$

Where D_A and D_B are the concentration of simvastatin and AZD6244 used in combination to achieve X % drug effect. $IC_{X,A}$ and $IC_{X,B}$ are the concentrations of simvastatin and AZD6244 as single agents to achieve the same effect. A CI of less than 1 indicates synergy.

Real-time quantitative PCR

RNA was extracted using the RNAeasy kit (QIAGEN) and cDNA synthesized using QuantiTect Reverse Transcription Kit (QIAGEN). SYBR Green Master Mix (Bio-Rad) was used to prepare PCR reaction mixtures containing 1 µg of cDNA. A CFX96 thermal cycler (Bio-rad) was used to perform the PCR reaction. Tubulin was used as a reference gene for mouse and actin for human samples.

DCFDA assay

2′, 7′-Dichlorofluorescin diacetate (DCFDA) was used to measure intracellular ROS using the DCFDA Cellular ROS Detection Assay Kit (ab113851, AbCam) according to the manufacturer's protocol. Cells were treated for 24 h in the indicated conditions prior to assay in base media containing 5% dFBS, 10 mM glucose and 2 mM glutamine and indicated drugs/DMSO with no phenol red. A Tecan SPARK plate

reader with excitation/emission wavelengths filter: 490/510–570 nm was used to detect fluorescence. Average relative fluorescence of control was equated to 100%, with treatment conditions calculated proportionally. Signal was background corrected and adjusted to cell number.

Immunohistochemistry

Immunohistochemistry of formalin-fixed paraffin-embedded tumor and benign pancreas blocks was obtained from cohort mice treated with vehicle, simvastatin or simvastatin + AZD6244. Phospho-Histone H2A.X (Ser139) (20E3) (ɣH2AX) (Cell Signalling), at 1:50 dilution, anti-8-Hydroxy-2'-deoxyguanosine (N45.1) (s-hydroxy) (AbCam) at 1:200 dilution, Caspase-3 (Cell Signaling) at 1:500 dilution primary antibodies were used. Antigens were retrieved in a PT Module (Agilent) for 25 min at 98^{o}C in PT Module 1 buffer (Thermo, UK). For Phospho-Histone H2A.X and caspase-3 endogenous peroxidase activity was blocked by incubation with 3% H_2O_2. This step was carried out after anti-8-Hydroxy-2'-deoxyguanosine staining, so as not to disrupt ROS. Staining was performed on a Dako Autostainer Link48 (for s-hydroxy and ɣH2AX) and a Leica Bond RX Autostainer (Caspase-3) with the primary antibody applied for 45 min at room temperature and 30 min, respectively. Sections were washed with Tris Buffered Tween (TbT) and Rabbit EnVision (Agilent, UK) was applied for 30 min, before washing with TbT and then application of Liquid DAB (Agilent, UK) for 10 min. Sections were rinsed in water on an autostainer and counterstained with Haematoxylin, nuceli blue'd, before being dehydrated and cleared through graded alcohols and xylene before application of a permanent coverslip.

Results

Statins only modestly affect cholesterol pools, but robustly block coenzyme Q synthesis in cancer cells

Cells acquire cholesterol either through uptake of lipoproteins from the extracellular environment, or by synthesizing it *de novo* (23) (Fig. 1A). In pancreatic and prostate cancer, cholesterol metabolism genes in particular have been shown to be deregulated (8,24). Cholesterol synthesis itself has not been measured before in these cancer types, and therefore we explored cholesterol dynamics as well as the effect of statins.

We performed a stable isotope tracing experiment with both [U^{13}C]-glucose and [U^{13}C]-glutamine in a cancer cell line derived from the KPC (Pdx1-Cre; Kras$^{G12D/+}$; Trp53$^{R172H/+}$) genetically engineered mouse model of pancreatic ductal adenocarcinoma (PDAC). In the presence of 5% (high) serum approximately 90% of the cholesterol remained unlabeled and very little ^{13}C accumulated in the 27-carbon molecule (Fig. 1B, S1A), thus indicating minimal *de novo* synthesis, but robust uptake of (unlabeled) cholesterol from the medium. As serum is a source of unlabeled cholesterol, we next lowered extracellular cholesterol by reducing serum to 2% (low) (Fig. 1B, S1A). While the fraction of unlabeled (M^0) cholesterol remained substantial, the presence of heavily ^{13}C-labeled isotopologs now demonstrated active cholesterol synthesis (Fig. 1B). Of note, we observed partially labeled molecules that contain both ^{12}C and ^{13}C. This is still indicative of complete *de novo* cholesterol synthesis, and is caused by partial labeling of the acetyl-CoA pool, which is also observed for other macro-molecules (25). Based on this labeling pattern, uptake (M^0) and synthesis (M^{14} – M^{27}) contributed roughly equally to the cholesterol pool (Fig. S1A). A similar observation was made in the human PDAC cell line MIA-

PaCa2 (Fig. S1B-D). These results demonstrate that cancer cells preferentially take up cholesterol from their extracellular environment, but can maintain cholesterol homeostasis by inducing *de novo* synthesis when extracellular availability is limited. This homeostasis is maintained during statin treatment (Fig. S1D); Simvastatin treatment in low serum conditions potently abrogated *de novo* cholesterol synthesis, but cells were still able adapt to maintain their cholesterol pool size by increasing cholesterol uptake (Fig. S1D-F).

By modulating serum availability during treatment of PDAC cell lines with simvastatin, we observed potent anti-proliferative effects in both high and low serum conditions (Fig. 1C, S1G). This finding was recapitulated with pitavastatin and atorvastatin, in KPC, MIA-PaCa2 and a human prostate cancer cell line, PC3 (Fig. S1G). As cholesterol synthesis is active in low serum but inactive in high serum, this suggests the anti-proliferative effect of statins is not mediated through inhibition of cholesterol metabolism. We therefore started exploring other branches of the mevalonate pathway (Fig. 1A). Using liquid chromatography – mass spectrometry (LC-MS)-based lipidomics, we were able to directly measure both dolichols and coenzyme Q (CoQ), also known as ubiquinone. Dolichols are composed of multiple concatenated 5-carbon isoprenoid units and function to ‘anchor’ glycosylation structures in membranes (26). CoQ is comprised of a benzoquinone ring derived from tyrosine, attached to a 9 (mouse, CoQ_9) or 10 (human, CoQ_{10}) isoprenoid-unit tail (Fig. 1D) (27). It functions as an electron carrier in the electron transport chain (ETC), and hence supports oxidative phosphorylation (2).

Analysis of dolichol labeling from [$U^{13}C$]-glucose and [$U^{13}C$]-glutamine revealed relatively little ^{13}C-incorporation, and hence a low rate of *de novo* synthesis (Fig. S1H). This contrasted with CoQ, which showed abundant ^{13}C-incorporation as

evidenced by the formation of a multitude of ^{13}C-labeled isotopologs (Fig. 1E). We confirmed that providing ^{13}C-labeled mevalonolactone, a routinely used cell permeable mevalonate analog that is rapidly converted upon entry into the cell, and tyrosine, also led to labeled CoQ (Fig. S1I-K). In all cell lines tested, statin treatment significantly reduced both *de novo* synthesis of CoQ and consequently CoQ pool size (Fig. 1F, 1G, S1L, M). It took 24 hours for statins to have a clear effect on CoQ levels, and this effect could be rescued using mevalonolactone (Fig. S1N). Together, these results demonstrate that, in contrast to cholesterol, CoQ is actively produced by cancer cells, and that both synthesis and pool size are reduced upon statin treatment.

Decreased CoQ levels cause impaired oxidative phosphorylation and a compensatory shift toward glycolysis

Succinate dehydrogenase (SDH), or complex II, participates both in the TCA cycle and the electron transport chain. It couples the oxidation of succinate with the reduction of CoQ (28). To establish whether diminished CoQ levels post statin treatment inhibited SDH activity, we determined the levels of its direct substrate succinate (Fig. 2A, S2A). Indeed, statin treatment caused significantly higher succinate levels, suggesting inhibition of SDH activity. We next asked if reduced SDH activity due to statin-mediated CoQ depletion more broadly impacted central carbon metabolism. We therefore measured oxygen consumption rate (OCR) after 24 hours of statin treatment, as CoQ depletion is strongest at this time (Fig. S1N). Simvastatin, pitavastatin and atorvastatin all reduced both basal and maximal respiration (Fig. 2B, S2B). Thus, reduced CoQ levels lowered oxidative phosphorylation (OXPHOS). Cells can compensate for loss of energy production

from the TCA cycle by increasing glycolysis. In accordance with this, we observed increased glucose uptake and lactate secretion (Fig. 2C, S2C). Of note, OXPHOS was restored upon mevalonolactone supplementation (Fig. S2D). Thus, cells switch to glycolysis to compensate for loss of OXPHOS-mediated ATP production due to statin-mediated CoQ depletion.

Statin-induced reduction in CoQ levels causes elevated ROS and activation of antioxidant metabolic pathways

Mitochondrial metabolism is intimately linked with ROS maintenance, and dysfunctional oxidative phosphorylation, as we observed with statin treatment (Fig. 2), can be a principal cause for excessive ROS generation (29). Additionally, the reduced form of CoQ, also known as ubiquinol, may have antioxidant functions in cells beyond oxidative phosphorylation (30). We next mined our metabolomics dataset to evaluate if oxidative stress occurs in statin treated cells. This revealed a striking shift in the ratio between oxidized and reduced glutathione towards the more oxidized form (Fig. 3A, S3A). Thus, it appears that oxidative stress is indeed a major consequence of statin treatment in cancer cells.

In recent years, multiple metabolic adaptations have been shown to have the ability to regulate redox balance (31). These adaptations include (I) the reductive formation of citrate from glutamine for shuttling NADPH into the mitochondria (32), (II) increased cellular cystine import for glutathione production (33), and (III) the synthesis of proline as an electron sink and ROS scavenger (34) (Fig 3B). Each of these pathways uses glutamine or derived metabolites as a substrate, and we therefore asked if glutamine uptake by statin treated cells was changed. Our analysis revealed a robust, roughly two-fold or higher increase in the rate by which glutamine

is taken up by statin treated cells, compared to untreated cells (Fig. 3C, S3B). While glutamate release also increased, it did not fully account for the increased uptake of glutamine, suggesting that statin treatment increases the rate by which glutamine-derived carbon feeds into downstream pathways.

We next investigated the effect of statin treatment on the activity of the aforementioned pathways that use glutamine as a substrate. Reductive citrate synthesis can be monitored using the M^{+5} isotopolog after feeding the cells [$U^{13}C$]-glutamine. In concordance with a change in central carbon metabolism and a potential role in redox management, the M^{+5} isotopolog and hence reductive carboxylation was robustly induced upon statin treatment (Fig. 3D, S3C). In addition, glutamine-derived glutamate can be exchanged with cystine via the cystine/glutamate antiporter SLC7A11/Slc7a11 (xCT) for glutathione production. Consistent with this pathway being active, glutamate secretion increased upon statin treatment, as did cystine uptake and intracellular cystine levels (Fig 3E, 3F, S3D, S3E). The transcript levels of *xCT* transporter also increased (Fig. 3G, S3F).

Finally, proline synthesis by pyrroline-5-carboxylate reductase (PYCR) from glutamine can also help regulate redox balance by regenerating NAD^+ which in turn may promote TCA cycling (35). Accordingly, we found that statin treatment robustly increased proline from glutamine (Fig. 3H, S3G). *PYCR1/Pycr1* transcript levels were also elevated (Fig. 3I, S3H). Proline itself can act as a ROS scavenger, reacting with hydroxyl radicals to form hydroxyproline (34,36). We indeed observed intracellular hydroxyproline levels to be significantly increased upon statin treatment (Fig. 3J, S3I). Thus, proline synthesis from glutamine helps to regenerate NAD^+ and facilitate ROS scavenging.

We next asked if the effects of statin-induced redox stress could be alleviated by mevalonolactone supplementation (Fig. 3G, 3I, S3A, S3C, S3E-I). Indeed, cell proliferation was rescued by mevalonolactone supplementation, as well as by the antioxidant N-acetyl cysteine addition (Fig. S3J). Of note, direct CoQ supplementation did not rescue cell growth, but this could have been caused by the precipitation of CoQ in the culture medium, and we were unable to confirm uptake or use by the cells. Nevertheless, the ability of N-acetyl cysteine to rescue the effect of simvastatin is further evidence that the depletion of CoQ and resulting oxidative stress is an important mechanism of statin-induced cell death. Overall, our results indicate that treating cancer cells with statins leads to pronounced oxidative stress and cells compensate by activating redox-induced metabolic pathways that mitigate ROS damage.

Statin treatment decreases CoQ synthesis and causes oxidative stress, *in vivo*

We next evaluated mevalonate pathway activity *in vivo* using $^{2}H_2O$ tracing, which enables persistent labeling of macromolecules (37,38). Pdx1-Cre; $Kras^{G12D/+}$; $Trp53^{R172H/+}$ (KPC) mice were administered a 0.035 mL/g mouse weight $^{2}H_2O$ bolus to mice with palpable tumors, followed by exposure to 8% $^{2}H_2O$ in drinking water for 7 days, which consistently led to approximately 5% deuterium enrichment in plasma (Fig. S4A).

We assessed ^{2}H-enrichment in cholesterol. A fractional enrichment of approximately 0.45 was observed in both liver and plasma of KPC mice (Fig. S4B, S4C). In healthy pancreas and tumors, the fractional enrichment of cholesterol was comparable to what was observed in plasma (Fig. S4D), suggesting that the *de novo* synthesis of cholesterol in tumors is minimal, as tumors actively take it up from the

bloodstream. Statin treatment had no significant impact on cholesterol labeling (Fig. S4C) or levels, which is consistent with reports that statins do not affect circulating blood cholesterol in mice, in contrast to in humans (39,40). Analysis of *in vivo* dolichol labeling revealed a similar labeling pattern to cholesterol, with labeling in tumors somewhat lower than in plasma, suggestive of minimal synthesis in the tumor, with no observable effect of simvastatin (Fig. S4E, S4F).

We next proceeded with analysis of CoQ. Notably, CoQ ^{2}H labeling in the small intestine was very high (fractional enrichment ~0.9), presumably due to the extremely rapid turnover of the epithelium (Fig. S4G). Fractional enrichment of circulating CoQ was strikingly similar to cholesterol (Fig. S4H). In contrast, while CoQ labeling in healthy pancreas was lower than circulating CoQ, the inverse was true in KPC PDAC tumors, where enrichment was significantly higher (Fig. 4A). As the enrichment is higher than circulating CoQ, this indicates active synthesis in the tumor. This was significantly reduced upon statin treatment (Fig. 4A). Notably, plasma CoQ_9 levels were not significantly altered by statin treatment, indicating a tumor specific effect (Fig. S4I), which appears in contrast to studies in healthy humans (41). Nevertheless, we conclude that PDAC tumors actively synthesize CoQ, and this synthesis is reduced by statin treatment.

We next wanted to investigate whether simvastatin treated tumors also had elevated ROS levels. Indeed, our immunohistochemistry demonstrated elevated oxidative damage, as there was significantly greater staining of ɣH2AX in the simvastatin treated cohort (Fig. 4B). We used 8-hydroxyguanosine as a DNA damage marker (42), and found significantly more stained cells in the simvastatin treated cohort than vehicle treated (Fig. S4J). Consistent with the metabolic compensation observed *in vitro*, we found that metabolic compensation to mitigate

oxidative stress occurred in the PDAC tumors. Specifically, we observed a significant increase in *xCT* (*Slc7a11*) transcript levels (Fig. 4C). Thus, simvastatin treatment leads to increased tumor ROS and tumors compensate by attempting to elevate glutathione production via *xCT* upregulation.

Combined statin and MEK inhibitor treatment synergize to accumulate ROS and cause apoptosis

Our findings revealed that statins reduce CoQ levels, causing oxidative stress, and metabolic compensation occurs to mitigate the effects of ROS damage. We next asked if disrupting these metabolic adaptations, together with statin treatment, would synergize to induce tumor cell death. The most pronounced metabolic adaptation we observed *in vivo* was upregulation of the *xCT* transporter (Fig. 4C). It was previously shown that the MEK inhibitor AZD6244 can promote ROS via NRF2 activation (43). In line with this, we found simvastatin treatment increased NRF2 transcript levels, whilst AZD6244 treatment reduced NRF2 transcript levels, as expected (Fig. S5A). As xCT is a NRF2 target (44) and NRF2 itself is regulated by MEK (45), we sought to determine if the ROS promoting effect of AZD6244 was through lowered expression of *xCT*. Indeed, AZD6244 was able to reduce *xCT* transporter levels in cultured cancer cells (Fig. 5A). We further validated this by testing MEK targets and found them to be reduced (Fig. S5B). Specifically, our previous results showed simvastatin elevates *xCT* mRNA levels, but in combination with AZD6244 this was prevented and the expression even reduced below the vehicle condition (Fig. 5A). This resulted in reduced cystine uptake (Fig. S5C), indicating that cells were not able to compensate for the elevated ROS from simvastatin treatment through increased cystine uptake for glutathione synthesis. In accordance, ROS levels were

significantly increased using the combination treatment (Fig. 5B). There was also a trend towards increased glutathione oxidation after combination treatment (Fig. S5D). Overall the combination treatment exacerbates ROS levels. Importantly, proliferation was substantially reduced upon combination treatment and NRF2 knock-down (Fig. 5C, S5E, S5F). NRF2 KD reduced NRF2 target transcript levels, and most notably xCT levels (Fig. S5G). Combined these results suggest AZD6244 may be synergizing with simvastatin.

To explore the potential synergy of AZD6244 and simvastatin further, the effect upon cell proliferation of the two drugs as single agents and in combination was analyzed (see Fig. S5H, S5I for example graphs). Using a matrix of all drug concentration combinations, the combination index (CI), as described by Chou-Talalay, was calculated (Fig. S5J, S5K). This demonstrated that the two drugs synergized at all except the very highest concentrations.

These results obtained *in vitro* led us to investigate the potency of a dual treatment of AZD6244 and simvastatin *in vivo*. We found the combination treatment reduced *in vivo xCT* transcript levels to well below the simvastatin treatment alone, and was comparable to the AZD6244 single-arm treatment (Fig. 5D). This shows AZD6244 is able to counter the elevated *xCT* levels induced by statin treatment in the tumor setting (Fig. 5E). Strikingly, our immunohistochemistry revealed caspase-3 induction and associated apoptotic body numbers were significantly higher in the combination treatment compared to vehicle, AZD6244 or simvastatin alone (Fig. 5F, 5G). Combined, these results indicate that a combined treatment with statin and a MEK inhibitor may be an effective cancer treatment paradigm.

Discussion

Our rationale for studying the mevalonate and downstream pathways in cancer was two-fold. First, while the mevalonate pathway is known to be upregulated in a number of different cancer types (6,8,10), and to be critical for tumorigenesis (9), what downstream products are synthesized and how they contribute to tumorigenesis, thus far remained largely unexplored. Second, despite the importance of the mevalonate pathway in cancer, the chemotherapeutic potential of the ubiquitously prescribed statins, either as a single agent or in a combination strategy, remained uncertain. We combined both GC-MS and LC-MS modalities with innovative stable isotope tracing approaches to determine the metabolic activity of this branch of metabolism, as well as the compensatory mechanisms that occur upon pharmacological inhibition.

It is well established that statins lower circulating cholesterol levels in humans, yet few studies have looked at cholesterol metabolism directly in cancers (8,46). Using tracers, we directly measured cholesterol metabolism, both *in vitro* and *in vivo,* to reveal that cancer cells preferentially take up cholesterol, rather than synthesizing it. Cholesterol uptake occurs via the LDL receptor and its increased expression has been reported in a variety of tumor types, including pancreatic cancer (8).

Although our labeling studies clearly demonstrated that cholesterol synthesis is minimal in tumor cells, statin treatment still elicited a robust anti-proliferative response. Through further exploration using an innovative combination of stable isotope tracing and lipidomics, we discovered that CoQ is actively synthesized by cancer cells. This contrasted with the synthesis of dolichols, which showed substantially less pronounced labeling. The principal function of CoQ is to act as an electron carrier in the electron transport chain (ETC), to facilitate mitochondrial

respiration. Apart from distinct oncogenic mutations and deletions in TCA cycle enzymes (47), mitochondrial metabolism is typically active in tumor cells and an important source for both energy and building blocks for macro-molecules (48). In fact, multiple recent reports demonstrated heightened glucose oxidation in tumors (49,50), stressing the importance of mitochondrial metabolism in cancer.

Statin-mediated CoQ depletion causes severe oxidative stress, which is likely caused by the disruption in mitochondrial metabolism. A few reports have previously postulated a link between statins, reduced CoQ levels, and increased ROS in other cell types, and this has been suggested as a cause for statin-induced myopathy (51,52). However, the published data supporting this was circumstantial. We now establish this link in unprecedented detail and show it also occurs in cancer cells. Furthermore, we made the novel observation that statin-mediated CoQ depletion leads to the compensatory induction of multiple metabolic pathways, with each having a unique anti-oxidant role. Particularly pronounced in both *in vitro* and *in vivo* settings was the upregulated expression of the *xCT* transporter. This has previously been shown to occur in response to oxidative stress by helping cells to obtain cystine needed for glutathione production (53). Of note, the statin mediated effect on ROS through CoQ is distinctly different from recent reports on squalene, which accumulates in some cancers and has an antioxidant function (54,55).

Our study highlights the capability of statins to inhibit CoQ synthesis. However, we recognize that this may not be the sole chemotherapeutic effect of statins. Multiple elegant reports have highlighted the pronounced effect of statins on protein prenylation, a post-translational modification that occurs on prominent oncoproteins, including members of the RAS family (56,57). Recent evidence, however, clearly demonstrated that the anticancer effects of statins is not due to

reduced RAS protein prenylation (12). Therefore, other statin-induced alterations, including the pronounced ROS production due to CoQ loss, contribute to its chemotherapeutic potential.

Statins, extensively prescribed for cardiovascular disease, have been widely evaluated for their effects on tumor development and progression, yet their clinical effect is variable (58–60). A phase II clinical trial of simvastatin and gemcitabine in PDAC patients found no clinical benefit to combining the statin with the only chemotherapy currently available for pancreatic cancer patients (61). Similarly for prostate cancer, a recent randomized double blind trial found no significant difference between atorvastatin and placebo (62). We explored statins in both pancreatic and prostate cancer cell lines, as well as an *in vivo* genetically engineered mouse model of PDAC. Both *in vitro* and *in vivo* simvastatin reduced CoQ synthesis significantly and tumors exhibited elevated ROS levels and *xCT* transcript levels. This led us to target the compensatory *xCT* upregulation using the MEK inhibitor AZD6244 and we found this dual combination with simvastatin induced apoptosis in the tumor. Our findings are directly relevant to unearthing a potential therapy for these cancers by hitting the cancers metabolic ROS compensatory mechanism to statin action.

We urgently need better treatments to target aggressive cancers such as PDAC, for which therapeutic options are currently very limited. We have used two FDA approved drugs and demonstrated their synergy and potential as a combinatorial cancer therapy.

Acknowledgments

The authors thank Vinay Bulusu for comments on the manuscript, Karen Blyth for using her animal license (70-8645), and Jennifer Morton for help with the *in vivo* work. The authors thank AstraZeneca for providing the AZD6624 compound.

Funding

Cancer Research UK Career Development Fellowship (C50242/A17728): J.J.K., S.T.

Cancer Research UK Grant (A17196): G.H.M., O.J.S., A.D.C., S.F.

Rosetrees Trust (M480): G.H.M

Cancer Research UK Beatson Institute (C596/A17196) and Cancer Research UK Glasgow Centre (C596/A18076): D.S., G.R.B., C.N., A.V

Bibliography

1. Zhang FL, Casey PJ. Protein Prenylation: Molecular Mechanisms and Functional Consequences. *Annu Rev Biochem* **1996**;65:241–69.
2. Brandt U. Proton translocation in the respiratory chain involving ubiquinone--a hypothetical semiquinone switch mechanism for complex I. *Biofactors* **1999**;9:95–101.
3. Goldstein JL, Brown MS. Regulation of the mevalonate pathway. *Nature* **1990**;343:425–30.
4. Nelson RH. Hyperlipidemia as a risk factor for cardiovascular disease. *Prim Care* **2013**;40:195–211.
5. Davidson MH. Safety profiles for the HMG-CoA reductase inhibitors: treatment and trust. *Drugs* **2001**;61:197–206.
6. Clendening JW, Pandyra A, Boutros PC, El Ghamrasni S, Khosravi F, Trentin GA, et al. Dysregulation of the mevalonate pathway promotes transformation. *Proc Natl Acad Sci* **2010**;107:15051–6.
7. Larson RA, Yachnin S. Mevalonic acid induces DNA synthesis in chronic lymphocytic leukemia cells. *Blood* **1984**;64:257–62.
8. Guillaumond F, Bidaut G, Ouaissi M, Servais S, Gouirand V, Olivares O, et al. Cholesterol uptake disruption, in association with chemotherapy, is a promising combined metabolic therapy for pancreatic adenocarcinoma. *Proc Natl Acad Sci* **2015**;112:2473–8.
9. Moon S-H, Huang C-H, Houlihan SL, Regunath K, Freed-Pastor WA, Morris JP, et al. p53 Represses the Mevalonate Pathway to Mediate Tumor Suppression. *Cell* **2019**;176(3):564-580
10. Harshman LC, Wang X, Nakabayashi M, Xie W, Valenca L, Werner L, et al.

Statin Use at the Time of Initiation of Androgen Deprivation Therapy and Time to Progression in Patients With Hormone-Sensitive Prostate Cancer. *JAMA Oncol* **2015**;1:495.

11. Chae YK, Valsecchi ME, Kim J, Bianchi AL, Khemasuwan D, Desai A, et al. Reduced Risk of Breast Cancer Recurrence in Patients Using ACE Inhibitors, ARBs, and/or Statins. *Cancer Invest* **2011**;29:585–93.
12. Yu R, Longo J, van Leeuwen JE, Mullen PJ, Ba-Alawi W, Haibe-Kains B, et al. Statin-Induced Cancer Cell Death Can Be Mechanistically Uncoupled from Prenylation of RAS Family Proteins. *Cancer Res* **2018**;78:1347–57.
13. Hingorani SR, Wang L, Multani AS, Combs C, Deramaudt TB, Hruban RH, et al. Trp53R172H and KrasG12D cooperate to promote chromosomal instability and widely metastatic pancreatic ductal adenocarcinoma in mice. *Cancer Cell* **2005**;7:469–83.
14. Lewis CA, Parker SJ, Fiske BP, McCloskey D, Gui DY, Green CR, et al. Tracing Compartmentalized NADPH Metabolism in the Cytosol and Mitochondria of Mammalian Cells. *Mol Cell* **2014**;55:253–63.
15. McCabe BJ, Bederman IR, Croniger C, Millward C, Norment C, Previs SF. Reproducibility of gas chromatography–mass spectrometry measurements of 2H labeling of water: Application for measuring body composition in mice. *Anal Biochem* **2006**;350:171–6.
16. Yang D, Diraison F, Beylot M, Brunengraber DZ, Samols MA, Anderson VE, et al. Assay of low deuterium enrichment of water by isotopic exchange with [U-13C3]acetone and gas chromatography-mass spectrometry. *Anal Biochem* **1998**;258:315–21.
17. Tumanov S, Bulusu V, Kamphorst JJ. Analysis of Fatty Acid Metabolism Using

Stable Isotope Tracers and Mass Spectrometry. *Methods Enzymol* **2015**;561:197–217.

18. Mackay GM, Zheng L, van den Broek NJF, Gottlieb E. Analysis of Cell Metabolism Using LC-MS and Isotope Tracers. *Methods Enzymol* **2015**;171–96.

19. Melamud E, Vastag L, Rabinowitz JD. Metabolomic Analysis and Visualization Engine for LC−MS Data. *Anal Chem* **2010**;82:9818–26.

20. Lee W-NP, Bassilian S, Lim S, Boros LG. Loss of regulation of lipogenesis in the Zucker diabetic (ZDF) rat. *Am J Physiol Metab* **2000**;279:E425–32.

21. Lee WN, Bassilian S, Ajie HO, Schoeller DA, Edmond J, Bergner EA, et al. In vivo measurement of fatty acids and cholesterol synthesis using D2O and mass isotopomer analysis. *Am J Physiol Metab* **1994**;266:E699–708.

22. Chou T-C, Talalay P. Quantitative analysis of dose-effect relationships: the combined effects of multiple drugs or enzyme inhibitors. *Adv Enzyme Regul* **1984**;22:27–55.

23. Faust JR, Goldstein JL, Brown MS. Synthesis of ubiquinone and cholesterol in human fibroblasts: Regulation of a branched pathway. *Arch Biochem Biophys* **1979**;192:86–99.

24. Ashida S, Kawada C, Inoue K. Stromal regulation of prostate cancer cell growth by mevalonate pathway enzymes HMGCS1 and HMGCR. *Oncol Lett* **2017**;14:6533–42.

25. Tumanov S, Bulusu V, Kamphorst JJ. Analysis of Fatty Acid Metabolism Using Stable Isotope Tracers and Mass Spectrometry. *Methods Enzymol* **2015**;197–217.

26. Chojnacki T, Dallner G. The biological role of dolichol. *Biochem J* **1988**;251:1–

9.

27. Crane FL. Biochemical Functions of Coenzyme Q_{10}. *J Am Coll Nutr* **2001**;20:591–8.

28. Tretter L, Patocs A, Chinopoulos C. Succinate, an intermediate in metabolism, signal transduction, ROS, hypoxia, and tumorigenesis. *Biochim Biophys Acta - Bioenerg* **2016**;1857:1086–101.

29. Sabharwal SS, Schumacker PT. Mitochondrial ROS in cancer: initiators, amplifiers or an Achilles' heel? *Nat Rev Cancer* **2014**;14:709–21.

30. Ernster L, Forsmark-Andrée P. Ubiquinol: an endogenous antioxidant in aerobic organisms. *Clin Investig* **1993**;71:S60-5.

31. Starkov AA. The role of mitochondria in reactive oxygen species metabolism and signaling. *Ann N Y Acad Sci* **2008**;1147:37–52.

32. Jiang L, Shestov AA, Swain P, Yang C, Parker SJ, Wang QA, et al. Reductive carboxylation supports redox homeostasis during anchorage-independent growth. *Nature* **2016**;532:255–8.

33. Meister A, Anderson ME. Glutathione. *Annu Rev Biochem* **1983**;52:711–60.

34. Alia, Mohanty P, Matysik J. Effect of proline on the production of singlet oxygen. *Amino Acids* **2001**;21:195–200.

35. Hollinshead KER, Munford H, Eales KL, Bardella C, Li C, Escribano-Gonzalez C, et al. Oncogenic IDH1 Mutations Promote Enhanced Proline Synthesis through PYCR1 to Support the Maintenance of Mitochondrial Redox Homeostasis. *Cell Rep* **2018**;22:3107–14.

36. Smirnoff N, Cumbes QJ. Hydroxyl radical scavenging activity of compatible solutes. *Phytochemistry* **1989**;28:1057–60.

37. Patton GM, Lowenstein JM. Measurements of fatty acid synthesis by

incorporation of deuterium from deuterated water. *Biochemistry* **1979**;18:3186–8.

38. Diraison F, Pachiaudi C, Beylot M. In vivo measurement of plasma cholesterol and fatty acid synthesis with deuterated water: Determination of the average number of deuterium atoms incorporated. *Metabolism* **1996**;45:817–21.

39. Choudhury RP, Carrelli AL, Stern JD, Chereshnev I, Soccio R, Elmalem VI, et al. Effects of Simvastatin on Plasma Lipoproteins and Response to Arterial Injury in Wild-Type and Apolipoprotein-E-Deficient Mice. *J Vasc Res* **2004**;41:75–83.

40. Sparrow CP, Burton CA, Hernandez M, Mundt S, Hassing H, Patel S, et al. Simvastatin has anti-inflammatory and antiatherosclerotic activities independent of plasma cholesterol lowering. *Arterioscler Thromb Vasc Biol* **2001**;21:115–21.

41. Ghirlanda G, Oradei A, Manto A, Lippa S, Uccioli L, Caputo S, et al. Evidence of plasma CoQ10-lowering effect by HMG-CoA reductase inhibitors: a double-blind, placebo-controlled study. *J Clin Pharmacol* **1993**;33:226–9.

42. Young O, Crotty T, O'Connell R, O'Sullivan J, Curran AJ. Levels of oxidative damage and lipid peroxidation in thyroid neoplasia. *Head Neck* **2009**;32

43. DeNicola GM, Karreth FA, Humpton TJ, Gopinathan A, Wei C, Frese K, et al. Oncogene-induced Nrf2 transcription promotes ROS detoxification and tumorigenesis. *Nature* **2011**;475:106–9.

44. Habib E, Linher-Melville K, Lin H-X, Singh G. Expression of xCT and activity of system xc− are regulated by NRF2 in human breast cancer cells in response to oxidative stress. *Redox Biol* **2015**;5:33–42.

45. Cheung KL, Lee JH, Shu L, Kim J-H, Sacks DB, Kong A-NT. The Ras

GTPase-activating-like protein IQGAP1 mediates Nrf2 protein activation via the mitogen-activated protein kinase/extracellular signal-regulated kinase (ERK) kinase (MEK)-ERK pathway. *J Biol Chem* **2013**;288:22378–86.

46. Warita K, Warita T, Beckwitt CH, Schurdak ME, Vazquez A, Wells A, et al. Statin-induced mevalonate pathway inhibition attenuates the growth of mesenchymal-like cancer cells that lack functional E-cadherin mediated cell cohesion. *Sci Rep* **2014**;4:7593.

47. Cardaci S, Zheng L, MacKay G, van den Broek NJF, MacKenzie ED, Nixon C, et al. Pyruvate carboxylation enables growth of SDH-deficient cells by supporting aspartate biosynthesis. *Nat Cell Biol* **2015**;17:1317–26.

48. Fan J, Kamphorst JJ, Rabinowitz JD, Shlomi T. Fatty Acid Labeling from Glutamine in Hypoxia Can Be Explained by Isotope Exchange without Net Reductive Isocitrate Dehydrogenase (IDH) Flux. *Mol Syst Biol.* **2013**;9:712.

49. Davidson SM, Papagiannakopoulos T, Olenchock BA, Heyman JE, Keibler MA, Luengo A, et al. Environment Impacts the Metabolic Dependencies of Ras-Driven Non-Small Cell Lung Cancer. *Cell Metab* **2016**;23:517–28.

50. Marin-Valencia I, Yang C, Mashimo T, Cho S, Baek H, Yang X-L, et al. Analysis of tumor metabolism reveals mitochondrial glucose oxidation in genetically diverse human glioblastomas in the mouse brain in vivo. *Cell Metab* **2012**;15:827–37.

51. Kettawan A, Takahashi T, Kongkachuichai R, Charoenkiatkul S, Kishi T, Okamoto1 T. Protective Effects of Coenzyme Q10 on Decreased Oxidative Stress Resistance Induced by Simvastatin. *J Clin Biochem Nutr* **2007**;40:194–202.

52. Beltowski J. Statins and Modulation of Oxidative Stress. *Toxicol Mech*

Methods **2005**;15:61–92.

53. Conrad M, Sato H. The oxidative stress-inducible cystine/glutamate antiporter, system x c − : cystine supplier and beyond. *Amino Acids* **2012**;42:231–46.

54. Mahoney CE, Pirman D, Chubukov V, Sleger T, Hayes S, Fan ZP, et al. A chemical biology screen identifies a vulnerability of neuroendocrine cancer cells to SQLE inhibition. *Nat Commun* **2019**;10:96.

55. Ge H, Zhao Y, Shi X, Tan Z, Chi X, He M, et al. Squalene epoxidase promotes the proliferation and metastasis of lung squamous cell carcinoma cells though extracellular signal-regulated kinase signaling. *Thorac Cancer* **2019**;10(3):428-436

56. Liao J, Chung YT, Yang AL, Zhang M, Li H, Zhang W, et al. Atorvastatin inhibits pancreatic carcinogenesis and increases survival in LSL-KrasG12D-LSL-Trp53R172H-Pdx1-Cre mice. *Mol Carcinog* **2013**;52:739–50.

57. Alizadeh J, Zeki AA, Mirzaei N, Tewary S, Rezaei Moghadam A, Glogowska A, et al. Mevalonate Cascade Inhibition by Simvastatin Induces the Intrinsic Apoptosis Pathway via Depletion of Isoprenoids in Tumor Cells. *Sci Rep* **2017**;7:44841.

58. Kawata S, Yamasaki E, Nagase T, Inui Y, Ito N, Matsuda Y, et al. Effect of pravastatin on survival in patients with advanced hepatocellular carcinoma. A randomized controlled trial. *Br J Cancer* **2001**;84:886–91.

59. Kwan ML, Habel LA, Flick ED, Quesenberry CP, Caan B. Post-diagnosis statin use and breast cancer recurrence in a prospective cohort study of early stage breast cancer survivors. *Breast Cancer Res Treat* **2008**;109:573–9.

60. Krens LL, Simkens LHJ, Baas JM, Koomen ER, Gelderblom H, Punt CJA, et al. Statin Use Is Not Associated with Improved Progression Free Survival in

Cetuximab Treated KRAS Mutant Metastatic Colorectal Cancer Patients: *PLoS One* **2014**;9:e112201.

61. Hong JY, Nam EM, Lee J, Park JO, Lee S-C, Song S-Y, et al. Randomized double-blinded, placebo-controlled phase II trial of simvastatin and gemcitabine in advanced pancreatic cancer patients. *Cancer Chemother Pharmacol* **2014**;73:125–30.

62. Murtola TJ, Syvälä H, Tolonen T, Helminen M, Riikonen J, Koskimäki J, et al. Atorvastatin Versus Placebo for Prostate Cancer Before Radical Prostatectomy—A Randomized, Double-blind, Placebo-controlled Clinical *Trial. Eur Urol* **2018**;74:697–701.

Figure 1. The cytostatic effect of statins is mediated through a decrease in coenzyme Q

(A) Schematic overview of the mevalonate pathway. (B) Cholesterol labeling distribution in KPC (Pdx1-Cre; $Kras^{G12D/+;}$ $Trp53^{R172H/+}$) cells incubated with [$U^{13}C$]-glucose and [$U^{13}C$]-glutamine fed for 72 h in either high serum (5% dFBS) or low serum (2% dFBS). Data has been corrected for ^{13}C natural abundance. The orange carbons on the cholesterol molecules represent ^{12}C and the purple carbons represent ^{13}C. (C) Effect of simvastatin (Simva) on cell proliferation in high and low serum. KPC and MIA-PaCa2 cells were treated with simvastatin in high (5%) or low (2%) serum for 48 h. Numbers are relative to vehicle (DMSO) treated control. (D) Schematic of CoQ (Coenzyme Q) biosynthesis using 5C (5 carbon) isoprene units from the mevalonate pathway. (E) CoQ labeling pattern from [$U^{13}C$]-glucose and [$U^{13}C$]-glutamine fed to KPC cells for 48 h. (F) Fraction newly synthesized CoQ in KPC cells in vehicle control (DMSO) and simvastatin treated cells after 48 h. (G) CoQ pool size in KPC cells treated with simvastatin for 48 h. Values are relative to control. All data shown as mean ± SEM of (B) 2 (C) 4, (D-G) 3 biological replicates, each performed in triplicate. Statistical significance was tested by ANOVA (C) and t-test (F) and (G). ****$p<0.0001$, **: $p<0.01$ Abbreviations: ns- non-significant. See also Figure S1.

Figure 2. Diminished CoQ levels lead to succinate accumulation, reduced oxidative phosphorylation, and increased glycolysis

(A) Effect of statins on succinate pool sizes in KPC, MIA-PaCa2 and PC3 cells. Peak areas were normalized to cell number and shown relative to vehicle control (DMSO). (B) Effect of statin treatment on oxidative phosphorylation. Cells were pre-treated

with vehicle control (DMSO) or simvastatin for 24 h prior to analysis. (C) Glucose uptake and lactate release rates in the media quantified after 48 h of simvastatin treatment. All data shown as mean ± SEM of (A) 3 or 1 (C) representative biological replicates, each experiment performed in triplicate, (B) 3 biological replicates each with 10 replicates. Abbreviations: OCR: Oxygen consumption rate, Rot/AA: rotenone and antimycin A. Statistical significance was tested by t-test. *: $p<0.05$, **: $p<0.01$ and ****$p<0.0001$. See also Figure S2.

Figure 3. Statin treatment causes increased redox stress and metabolic compensation.

(A) Effect of simvastatin (Simva) on the ratio of oxidized (GSSG) to reduced (GSH) glutathione (48 h). Relative to vehicle control (DMSO). (B) Overview of metabolic pathways mitigating oxidative stress. (C) Glutamine uptake and glutamate release rates in response to vehicle or simvastatin (2 μM). (D) Citrate labeling from [$U^{13}C$]-glutamine tracing for 48 h. (E) Change in cystine uptake in response to simvastatin treatment. Rates are relative to vehicle control. (F) Effect of simvastatin treatment on intracellular cystine levels (48 h). Values are relative to control. (G) qPCR analysis of *xCT* following statin treatment and statin plus mevalonolactone (Mev.) (48 h). (H) Proline labeling from [$U^{13}C$]-glutamine after statin treatment (48 h). Peak areas were normalized to cell number and expressed relative to control. (I) qPCR analysis of *PYCR1* after simvastatin treatment and statin plus mevalonolactone (Mev.) (48 h). (J) Intracellular hydroxyproline levels in response to statin treatment. Peak areas were normalized to cell numbers and expressed relative to control. All data shown as mean ± SEM of (A), (D), (F), (J) 3 biological replicates, each performed in triplicate, (C), (E), (H) 1 representative biological replicate, each

performed in triplicate, (G), (I) 3 biological replicates from 6 technical repeats. Statistical significance was tested by ANOVA for (G) and (I), rest by t-test. *: p<0.05, **: p<0.01, ***: p<0.001, ****p<0.0001. See also Figure S3.

Figure 4. Statin treated KPC mice have reduced tumor CoQ synthesis and pronounced oxidative stress.

(A) Fraction newly synthesized CoQ_9 in KPC PDAC tumors and benign adjacent pancreas. (B) Immunohistochemistry (IHC) and scoring of DNA damage response by ɣH2AX in tumor. Scale bar in larger image represents 50 µm, smaller image represents 20 µm. (C) qPCR analysis of *xCT* in PDAC tumors from KPC mice. For (A), (C) data shown as mean ± SEM for n = 4 mice per group. Note one vehicle mouse had no benign pancreas. For (B) quantification shown as median score ± SEM from 30 frames for n = 4 mice per group. Abbreviations: Panc: Pancreas, Veh: Vehicle. Statistical significance was tested by student's t-test for (A), (C) and Mann-Whitney (B). *:p<0.05, **: p<0.01 and ****p<0.0001. See also Figure S4.

Figure 5. A MEK inhibitor (AZD6244) synergizes with statin treatment to induce cell death due to excessive ROS.

(A) qPCR analysis of *xCT* expression following 48 h treatment with simvastatin, AZD6244 or combination. (B) Intracellular ROS as measured by DCFDA assay after 24 h treatment with simvastatin, AZD6244 or a combination. (C) Cell numbers following 96 h exposure to indicated conditions. Numbers are relative to vehicle (DMSO) treated control. (D) qPCR analysis of *xCT* (*Slc7a11*) expression in KPC PDAC tumors. (E) Schematic to show AZD6244 action reducing *xCT* level. (F) Caspase-3 IHC and scoring of KPC mice treated with vehicle control, simvastatin,

AZD6244 or AZD6244 + simvastatin. (G) H&E IHC and scoring of apoptotic bodies in KPC mice treated as in (F). Arrows indicate apoptotic bodies. For images, scale bar in larger image represents 50 µm, smaller image represents 20 µm. Data shown as mean ± SEM of (A) 3 biological replicates with each 6 technical replicates, (B) 3 biological replicates, with each 8 technical replicates, (C) 3 biological replicates, each performed in triplicate, (D), (F), (G) data is shown for n = 4 mice per group. (F), (G) quantification shown as median score ± SEM from 20 frames. Statistical significance was tested by ANOVA for (A), (B), (C), (D) or Mann-Whitney for (F), (G). *: $p<0.05$, **: $p<0.01$, ***: $p<0.001$, ****$p<0.0001$. See also Figure S5.

Figure 1

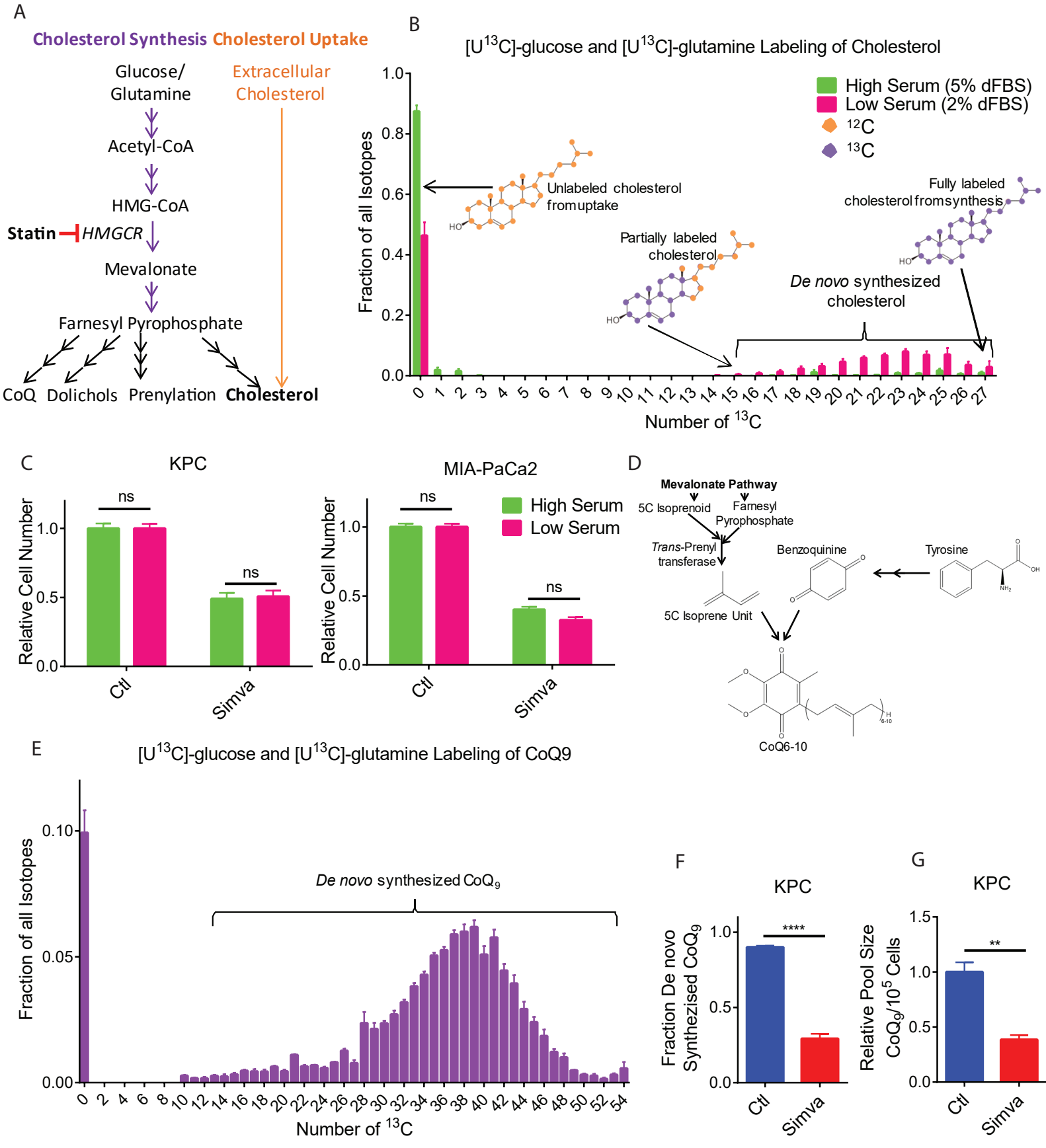
A
Cholesterol Synthesis
Cholesterol Uptake
Glucose/ Glutamine
Extracellular Cholesterol
Acetyl-CoA
HMG-CoA
Statin
HMGCR
Mevalonate
Farnesyl Pyrophosphate
CoQ
Dolichols
Prenylation
Cholesterol
B
[U13C]-glucose and [U13C]-glutamine Labeling of Cholesterol
High Serum (5% dFBS)
Low Serum (2% dFBS)
12C
13C
Fraction of all Isotopes
Unlabeled cholesterol from uptake
Partially labeled cholesterol
Fully labeled cholesterol from synthesis
De novo synthesized cholesterol
Number of 13C
C
KPC
MIA-PaCa2
Relative Cell Number
ns
High Serum
Low Serum
Ctl
Simva
D
Mevalonate Pathway
5C Isoprenoid
Farnesyl Pyrophosphate
Trans-Prenyl transferase
Benzoquinine
Tyrosine
5C Isoprene Unit
CoQ6-10
E
[U13C]-glucose and [U13C]-glutamine Labeling of CoQ9
Fraction of all Isotopes
De novo synthesized CoQ9
Number of 13C
F
KPC
Fraction De novo Synthesized CoQ9
****
G
KPC
Relative Pool Size CoQ9/10^5 Cells
**

Figure 2

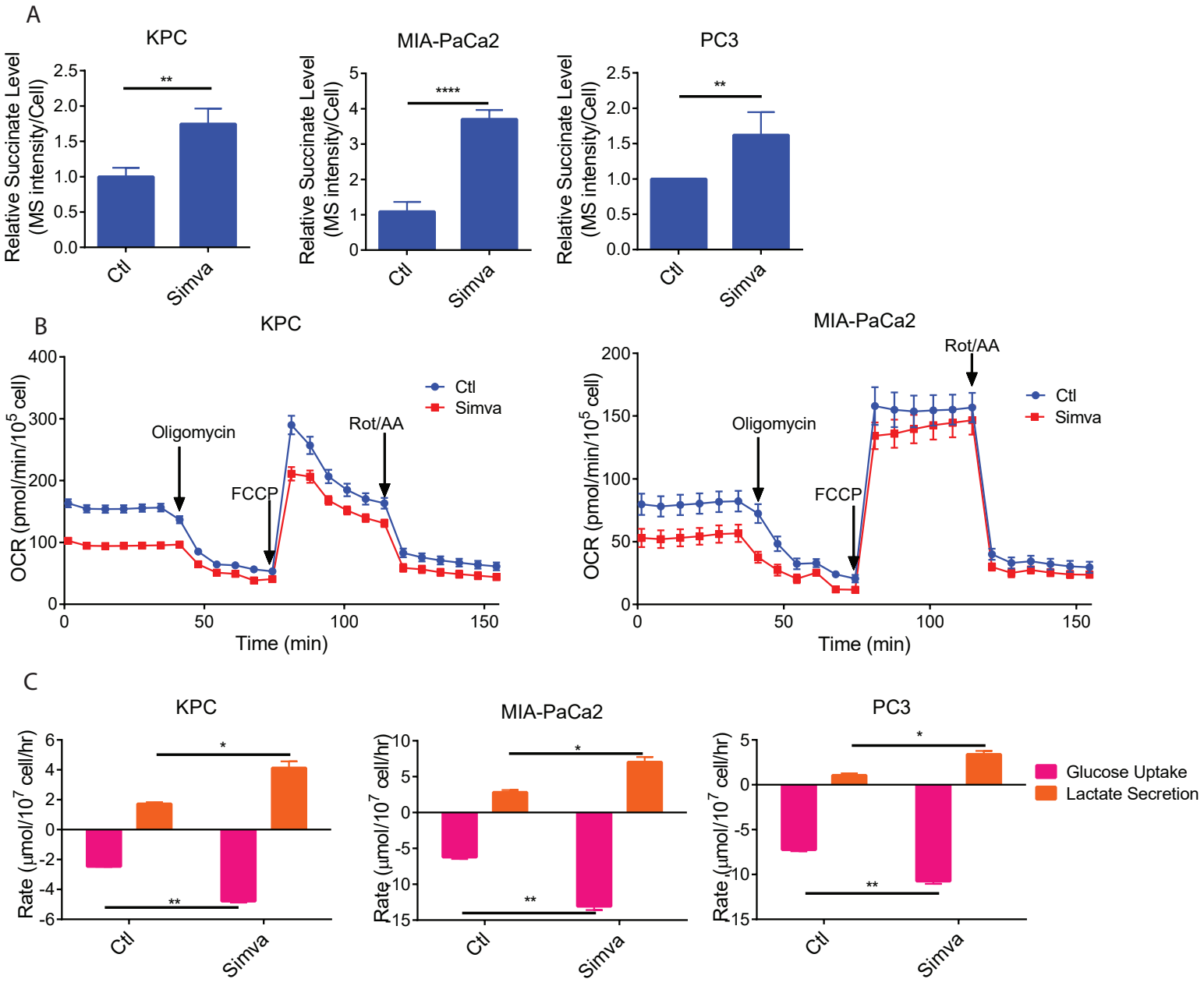
A
KPC
MIA-PaCa2
PC3
Relative Succinate Level (MS intensity/Cell)
Ctl
Simva
B
KPC
MIA-PaCa2
OCR (pmol/min/10^5 cell)
Oligomycin
FCCP
Rot/AA
Time (min)
C
Rate (μmol/10^7 cell/hr)
Glucose Uptake
Lactate Secretion

Figure 3

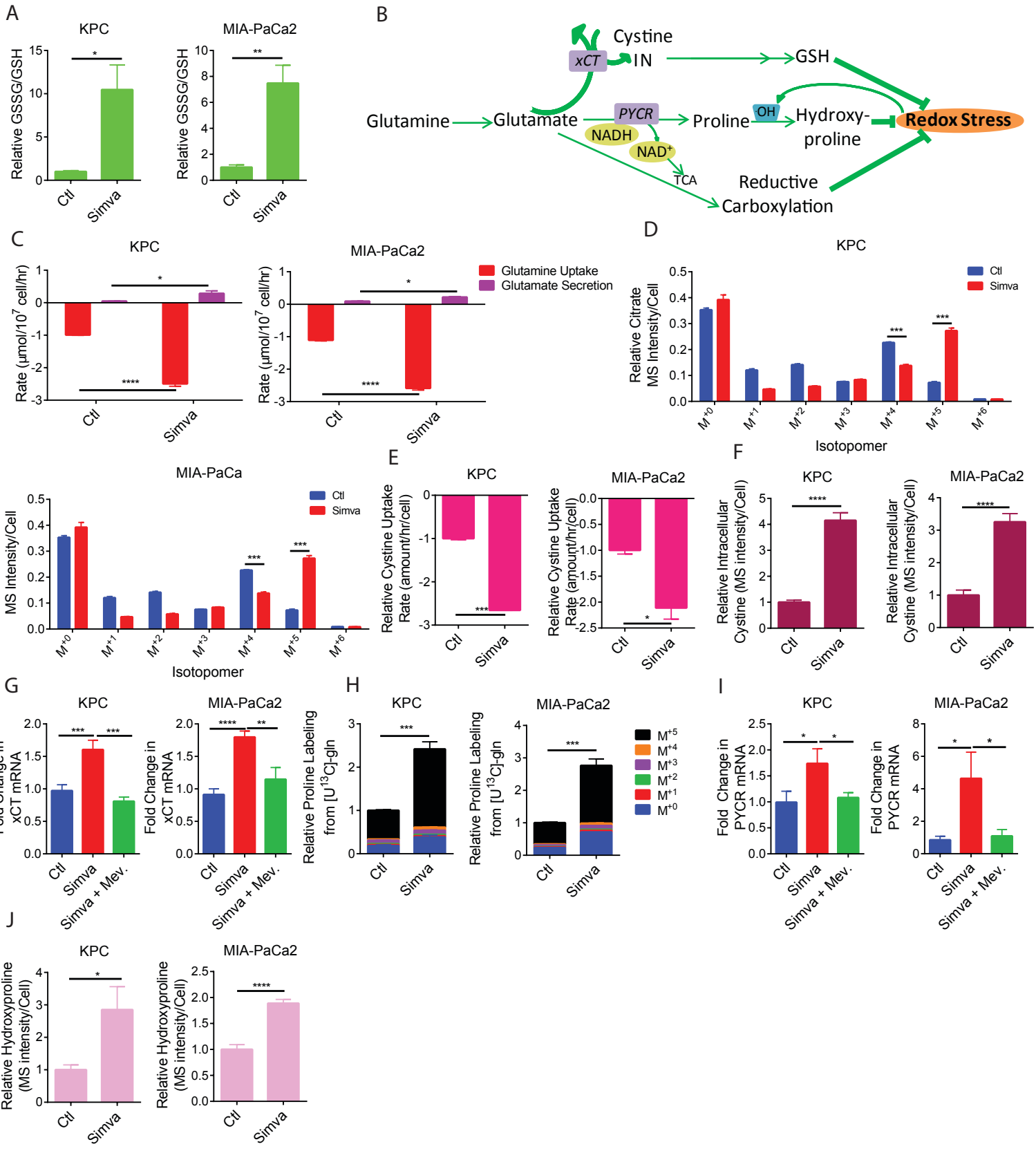
A
KPC
MIA-PaCa2
Relative GSSG/GSH
Ctl
Simva
B
Cystine
xCT
IN
GSH
Glutamine
Glutamate
PYCR
Proline
OH
Hydroxy-proline
Redox Stress
NADH
NAD+
TCA
Reductive Carboxylation
C
KPC
MIA-PaCa2
Rate (μmol/10^7 cell/hr)
Glutamine Uptake
Glutamate Secretion
D
KPC
MIA-PaCa
Relative Citrate MS Intensity/Cell
Isotopomer
E
KPC
MIA-PaCa2
Relative Cystine Uptake Rate (amount/hr/cell)
F
KPC
MIA-PaCa2
Relative Intracellular Cystine (MS intensity/Cell)
G
KPC
MIA-PaCa2
Fold Change in xCT mRNA
Simva + Mev.
H
KPC
MIA-PaCa2
Relative Proline Labeling from [U13C]-gln
I
KPC
MIA-PaCa2
Fold Change in PYCR mRNA
J
KPC
MIA-PaCa2
Relative Hydroxyproline (MS intensity/Cell)

Figure 4

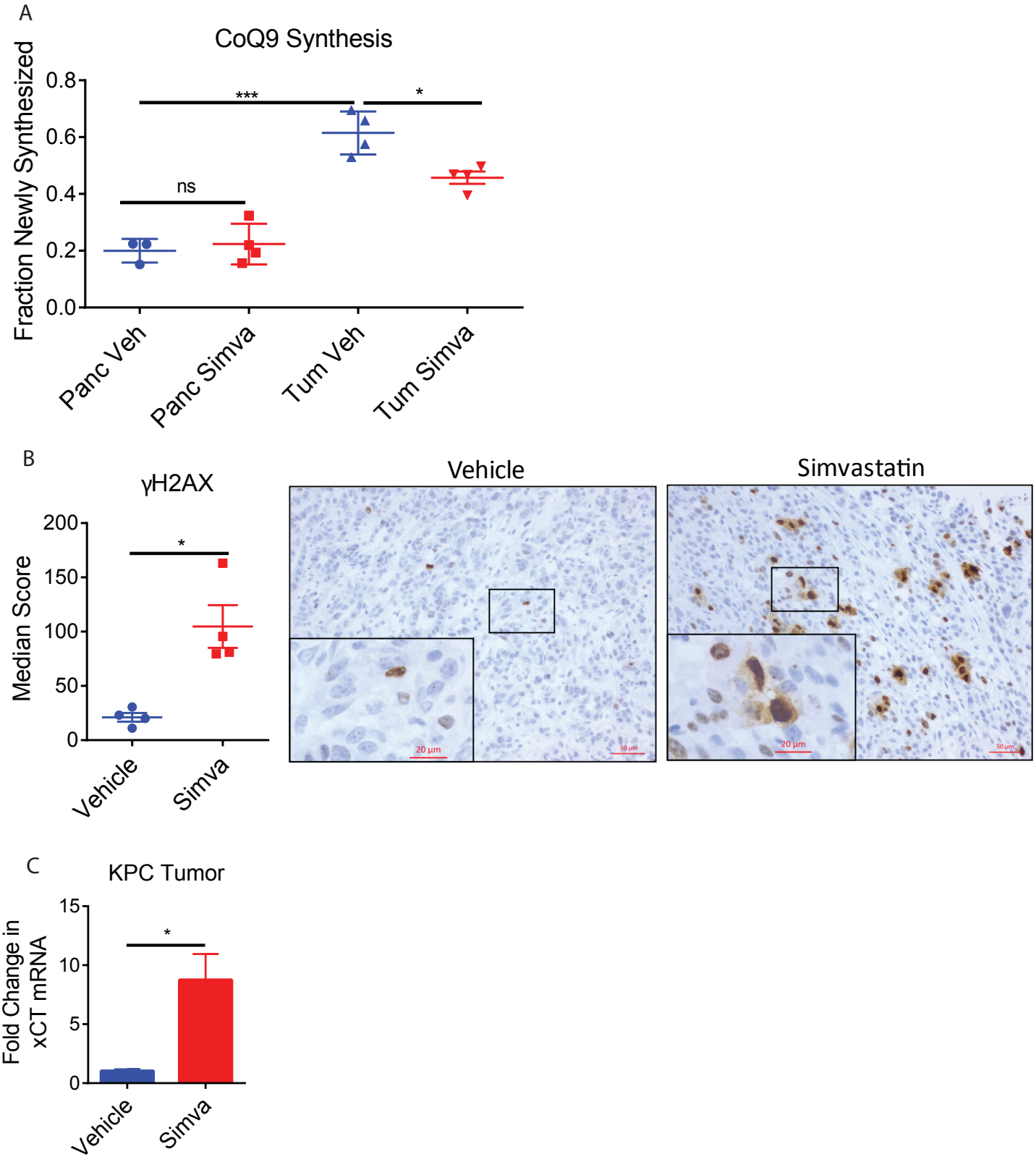
A
CoQ9 Synthesis
Fraction Newly Synthesized
0.8
0.6
0.4
0.2
0.0
***
*
ns
Panc Veh
Panc Simva
Tum Veh
Tum Simva
B
γH2AX
Median Score
200
150
100
50
0
*
Vehicle
Simva
Vehicle
Simvastatin
20 μm
50 μm
C
KPC Tumor
Fold Change in xCT mRNA
15
10
5
0
*
Vehicle
Simva

Figure 5

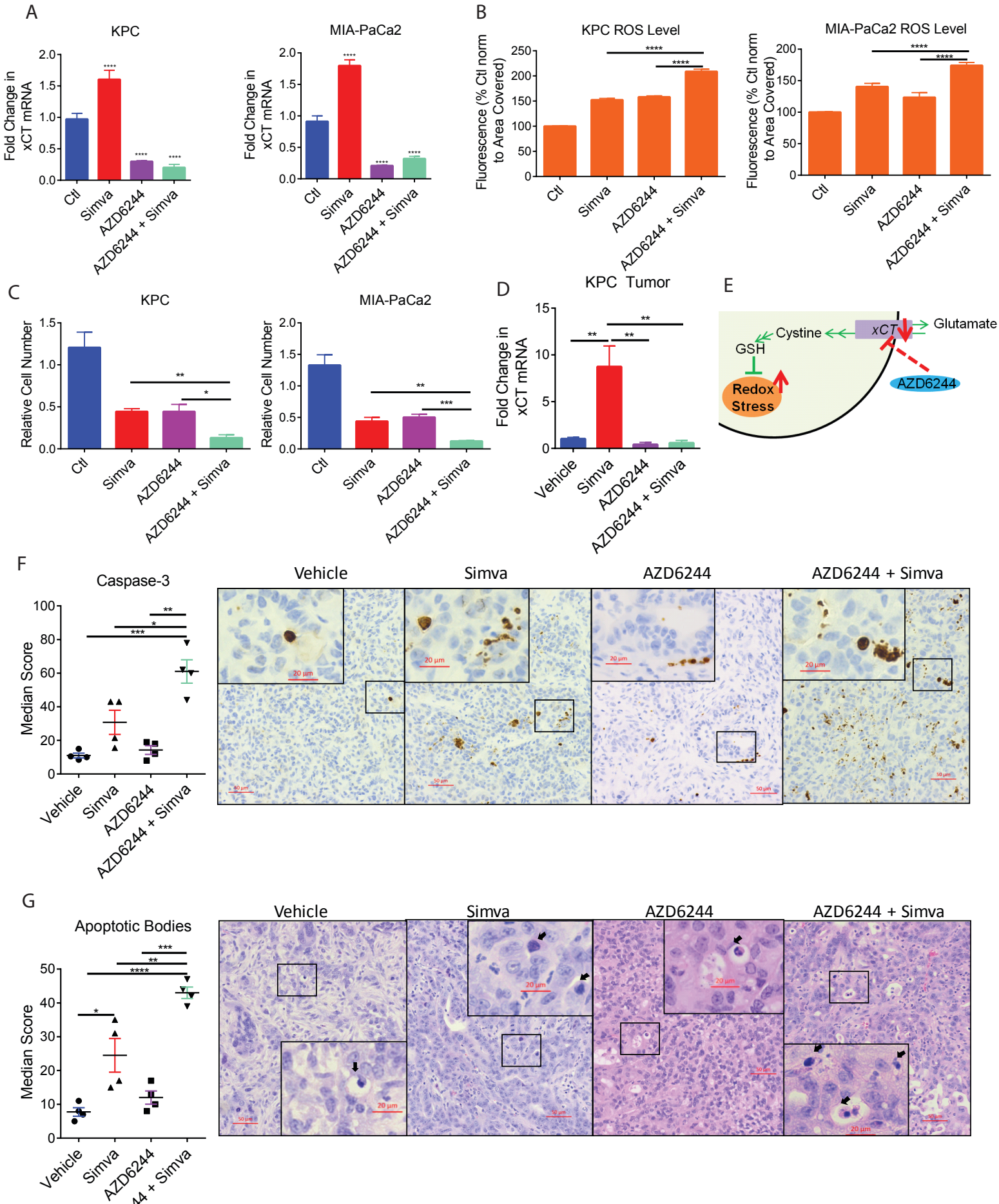
A
KPC
MIA-PaCa2
Fold Change in xCT mRNA
Ctl
Simva
AZD6244
AZD6244 + Simva
B
KPC ROS Level
MIA-PaCa2 ROS Level
Fluorescence (% Ctl norm to Area Covered)
C
KPC
MIA-PaCa2
Relative Cell Number
D
KPC Tumor
Vehicle
E
Cystine
xCT
Glutamate
GSH
Redox Stress
AZD6244
F
Caspase-3
Median Score
Vehicle
Simva
AZD6244
AZD6244 + Simva
G
Apoptotic Bodies